Semi-Annual Progress Report

on

SUPERSONIC CO ELECTRIC-DISCHARGE LASERS

NASA Grant NSG-2050

for the period

May 1, 1975 - October 31, 1975

Submitted to the

National Aeronautics and Space Administration

Washington, D. C.

by

Professor R. K. Hanson

Professor M. Mitchner

Mr. Alan Stanton

High Temperature Gasdynamics Laboratory

Department of Mechanical Engineering

Stanford University

Stanford, California 94305

TABLE OF CONTENTS

LIST OF FIGURES

1.0 SUMMARY

This report describes work carried out on NASA Grant NSG-2050 during the period May 1, 1975, to October 31, 1975. Our laser modeling activity has involved addition of an option to the current program, CØED 2, allowing N_2 as a second diatomic gas. This option is now operational and a few test cases involving N_2/CO mixtures have been run. Results from these initial test cases are summarized in this report.

In the laboratory, a new CW double-discharge test facility has been constructed and tested. New features include: water-cooled removable electrodes, O-ring construction to facilitate cleaning and design modifications, increased discharge length, and addition of a post-discharge observation section. Preliminary tests with this new facility using N_2 have already yielded higher power loadings than obtained in our first-generation facility. At present, power loading is limited by the power supply available, but a larger supply is on order and will be installed shortly. Another test-section modification, recently made and as yet untested, will permit injection of secondary gases into the cathode boundary layer. The objective here will be to vary and hopefully enhance the uv emission spectrum from the auxiliary discharge, thereby influencing the level of photoionization in the main discharge region.

2.0 LASER MODELING

2.1 Probabilities for V-V Exchange in CO-N_2 and N_2-N_2 Systems

2.1.1 CO-N_2 V-V Probabilities

Calculations of vibrational-vibrational energy exchange probabilities in pure CO are usually based on the assumption of independent contributions from short range and long range forces. The long range contribution is due to multipole-multipole interactions [1], of which the dipole-dipole term is dominant. The short range contribution arises from coulombic repulsive forces.

For molecular systems involving N_2, which has no permanent dipole moment, long range contributions are usually neglected in calculating V-V exchange probabilities. In models of vibrational kinetic processes in CO lasers, the CO-N_2 V-V probabilities are typically calculated with the short-range expression used for the pure CO calculation [2,3] with some modification to obtain agreement with experimental data. An expression of this type, based on the Schwartz-Slawsky-Herzfeld theory, was discussed in an earlier progress report.* Attempts to use this expression in calculating CO-N_2 probabilities, however, led to poor agreement with experimental results in either the vibrational quantum number dependence or the temperature dependence of the V-V probabilities. Much better agreement was obtained by abandoning the SSH theory and using in its place an expression obtained by an extension of the theory of H. K. Shin [4]. The

---

*Supersonic CO Electric Discharge Lasers, NASA Grant NSG-2050, Semi-annual Progress Report for the period November 1, 1974 - April 30, 1975.

remainder of this section is a brief discussion of Shin's theory and its extension, with comparisons with experimental data.

The theory is a semiclassical treatment, assuming harmonic oscillator wave functions and a three-dimensional classical collision trajectory. The overall interaction potential is assumed to be the sum of four atom-atom interaction potentials, which are represented by Morse functions. The interaction thus includes both attractive and repulsive terms. The molecules are assumed to be rotationless. A result is obtained only for the vibrational transitions involving the ground level and the first excited level, i.e., in the case of N_2 and CO, for the processes

$$N_2(v=1) + CO(v=0) \rightleftarrows N_2(v=0) + CO(v=1) \ .$$

For the forward process, Shin's result may be expressed in the form

$$P_{\substack{0,1 \\ 1,0}}^{(CO-N_2)} = (1.79\times10^{-2})\left(\frac{\chi}{kT}\right)^{1/2} \exp\left[\frac{-3\chi}{kT} + \frac{4(D\chi)^{1/2}}{\pi kT}\, g + \frac{16D}{3\pi^2 kT}\, g^2 + \frac{\hbar\omega}{2kT}\right] . \quad (1)$$

In this expression $\omega \equiv \omega_{N_2} - \omega_{CO}$ is the difference in vibrational frequencies of the two molecules, D is the well depth of the atom-atom interaction potentials, and g is a factor which arises in the particular formulation of the overall interaction potential. For the system of N_2 and CO, Shin's value for g is 0.712. The quantity χ in equation (1) is related to the difference in vibrational frequencies, as

$$\chi = \left[\left(\frac{\mu}{2}\right)^{1/2} \pi\omega a\ kT\right]^{2/3} \quad (2)$$

where μ is the reduced mass for the collision system and a is the range parameter in the interaction potentials. Shin's expression for the transition probability, equation (1), yields values which are in good agreement

with experimental data at both low and high temperatures [5].

Models of CO vibrational kinetics require a method of estimating the probabilities for single-quantum vibrational energy exchange involving any vibrational level. A simple means of extending Shin's result to the general V-V exchange reaction,

$$CO(v=r-1) + N_2(v=s) \rightleftarrows CO(v=r) + N_2(v=s-1) ,$$

is to assume harmonic oscillator scaling of the V-V probabilities, i.e.,

$$P_{\substack{r-1,r \\ s,s-1}} = rs\, P_{\substack{0,1 \\ 1,0}} \tag{3}$$

Equation (3) which follows from an assumption that the interaction Hamiltonian is independent of the initial states, is exact to second order in $P_{\substack{0,1 \\ 1,0}}$.

A further modification is to introduce anharmonicity effects by replacing $\hbar\omega$ in equation (1) with the actual energy nonresonance, $|\Delta E|^*$, and to correct the vibrational frequencies with anharmonicity factors:

$$\omega_{CO} = \omega_0^{(CO)}\left[1 - r\delta_{CO}\right] \tag{4}$$

$$\omega_{N_2} = \omega_0^{(N_2)}\left[1 - s\delta_{N_2}\right] . \tag{5}$$

These substitutions are ad hoc, and they are justified only by the better agreement with experimental data which is obtained.

---

*Note, however, that if this substitution is made in the pre-exponential term in equation (1), the probability for an exactly resonant V-V exchange would be zero. Although there are no exact resonances for purely vibrational transitions in CO and N_2, this perhaps academic difficulty is avoided by not making the substitution in the pre-exponential term.

A comparison of the probabilities calculated by the above method with the room-temperature data of Hancock and Smith [7] shows good agreement, although the calculated probabilities are generally larger by about a factor of two. Better agreement is obtained if the constant in the pre-exponential is chosen to fit the room-temperature data for $P_{\substack{0,1\\1,0}}^{(CO-N_2)}$.

The final expression for the probability for the single-quantum V-V reaction

$$CO(v=r-1) + N_2(v=s) \rightarrow CO(v=r) + N_2(v=s-1)$$

is then

$$P_{\substack{r-1,r\\s,s-1}}^{(CO-N_2)} = (3.52\times10^{-7}) \left[\frac{r}{1-r\delta_{CO}}\right]\left[\frac{s}{1-s\delta_{N_2}}\right] G(\chi;T) \exp\left(\frac{\Delta E}{2kT}\right). \tag{6}$$

The function $G(\chi;T)$ in this expression is defined as

$$G(\chi;T) = \left(\frac{\chi}{kT}\right)^{1/2} \cdot \frac{1}{|\Delta E|^{1/3}} \exp \frac{1}{kT}\left[\left(-3\chi + 4\frac{\sqrt{D\chi}}{\pi} g + \frac{16D}{3\pi^2} g^2\right)\right] \tag{7}$$

where

$$\chi = \left[(2\mu)^{1/2} \frac{a \pi^2 kT}{h} |\Delta E|\right]^{2/3} \tag{8}$$

and the energy nonresonance is given by

$$\Delta E = \left(E_s^{(N_2)} - E_{s-1}^{(N_2)}\right) - \left(E_r^{(CO)} - E_{r-1}^{(CO)}\right). \tag{9}$$

Equation (6) is the expression used to calculate the probabilities for $CO-N_2$ V-V exchange in CØED2. Following Shin, the values for the potential parameters used in these calculations are

$$a = 0.2\ \text{Å}$$

$$D = 1.385 \times 10^{-14}\ \text{ergs} .$$

Figures 1 and 2 are a comparison of the available low-temperature data [6-10] with the probabilities calculated from equation (6). Also plotted in these figures are the probabilities which would be obtained from the short-range SSH expression, with the constant in the pre-exponential chosen to match the room-temperature data for $P_{\substack{0,1\\1,0}}^{(CO-N_2)}$.

2.1.2 N_2-N_2 V-V Probabilities

A similar approach is taken to calculate the probabilities for V-V exchange in pure N_2. Shin's approach leads to a value of zero for exact resonance, so that in this case the process

$$N_2(v=0) + N_2(v=2) \rightarrow 2N_2(v=1)$$

is used as a basic process to which the vibrational quantum number scaling is applied. The calculation of the probability for this reference V-V process is the same as Shin's development for CO and N_2, although an additional factor of $\sqrt{2}$ appears in the evaluation of the scattering matrix element due to the choice of initial states. The extension to the general single-quantum V-V process,

$$N_2(v=r-1) + N_2(v=s) \rightarrow N_2(v=r) + N_2(v=s-1) ,$$

is made in exactly the same fashion as for the CO-N_2 probabilities.

The final result for the N_2-N_2 V-V probability is expressed by

$$P_{\substack{r-1,r\\s,s-1}}^{(N_2-N_2)} = (3.47\times10^{-9})\left[\frac{r}{1-r\delta_{N_2}}\right]\left[\frac{s}{1-s\delta_{N_2}}\right] G(\chi;T)\ \exp\left(\frac{\Delta E}{2kT}\right) . \qquad (10)$$

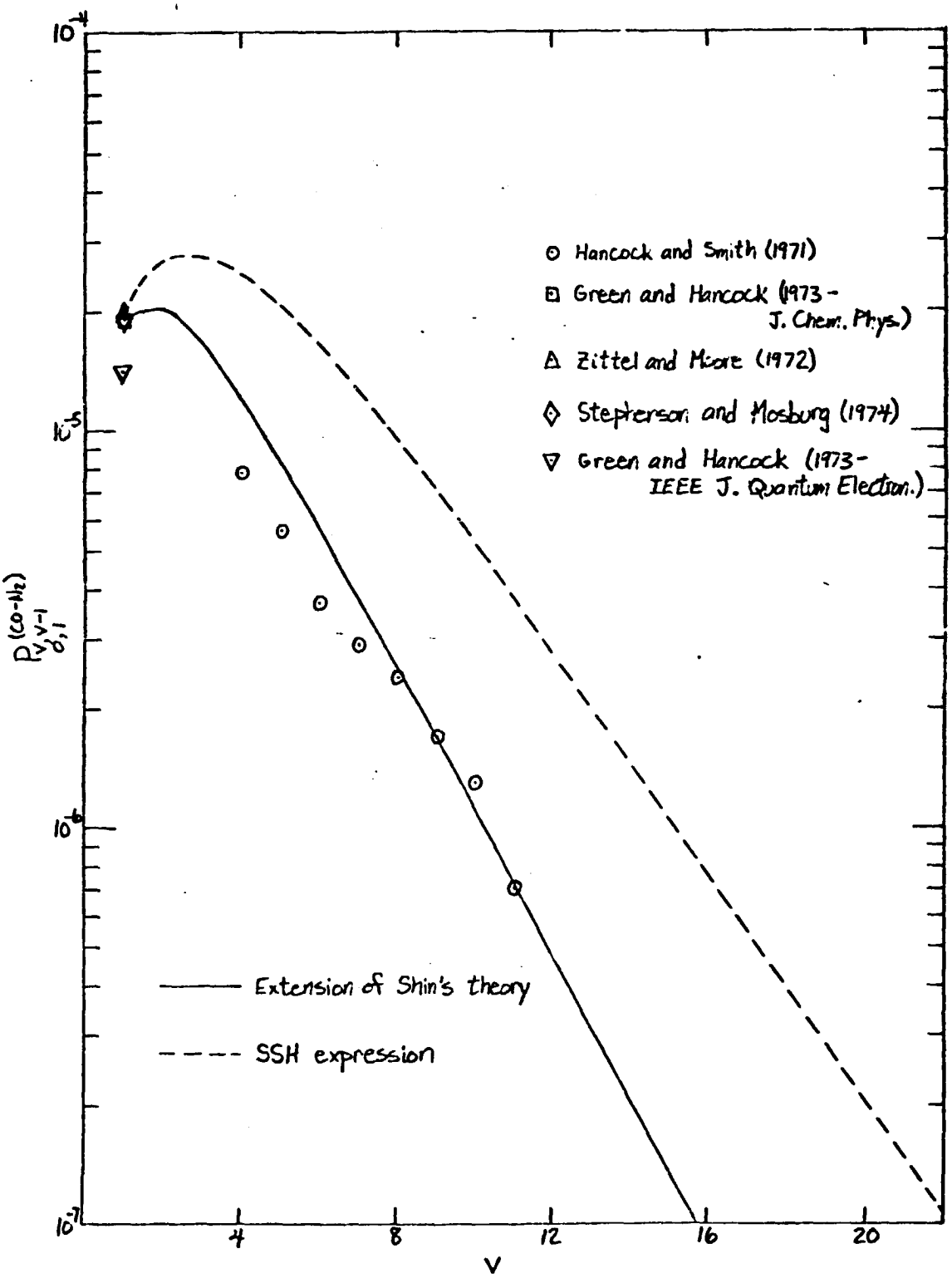

Figure 1. Room-temperature probabilities for the CO-N_2 V-V process CO(v) + N_2(v=0) → CO(v-1) + N_2(v=1). The calculated probabilities are fit to a value of 1.9×10^{-5} for $P^{(CO-N_2)}_{1,0}$ $\delta_{0,1}$

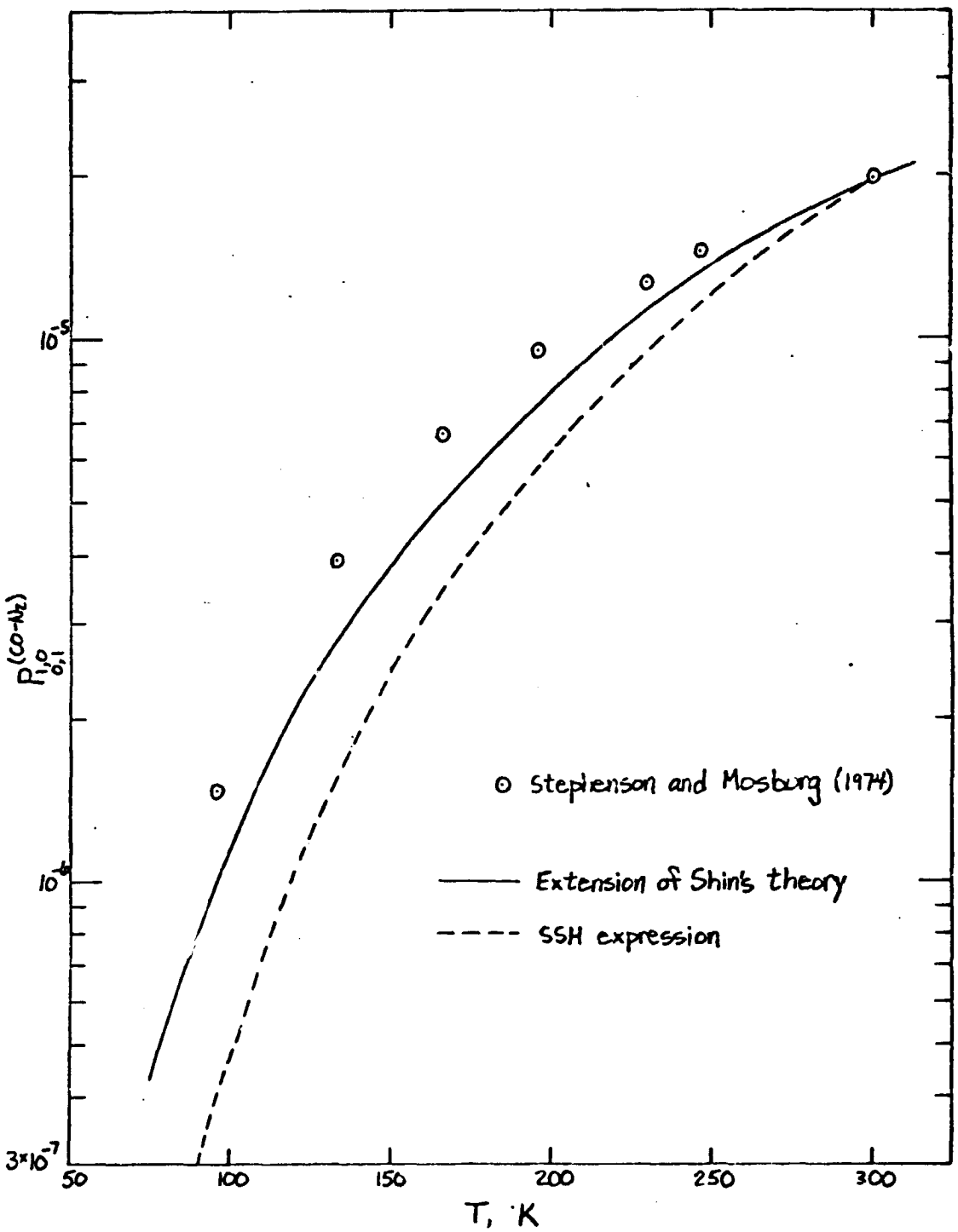

Figure 2. Comparison of the calculated probabilities with the low-temperature experimental results of Stephenson and Mcsburg for the V-V process. $CO(v=1) + N_2(v=0) \rightarrow CO(v=0) + N_2(v=1)$.

The definitions of the terms in this equation are the same as in equation (6) for the CO-N_2 case. The constant g has a value of 0.731 for N_2-N_2, and the values used for the potential parameters are

$$a = 0.2 \text{ Å}$$

$$D = 1.263 \times 10^{-14} \text{ ergs} .$$

Calculated probabilities for the V-V excitation of ground-level N_2 are plotted in Figure 3. The value calculated by Berend and Benson [11] for $P_{\substack{0,1 \\ 2,1}}^{(N_2-N_2)}$ at T = 300 K is also shown on this plot. Their calculation is based on a rigorous two-dimensional classical model, which includes the effects of molecular rotation and anharmonicity.

2.2 Calculations of CO/N_2 Laser Kinetics Using CØED2

With the inclusion of N_2 in the model of CO vibrational kinetics, CØED2 has become a useful tool in studying the relative importance of direct electron pumping and CO-CO and CO-N_2 V-V transfer processes in shaping the CO vibrational distribution in fast-flow continuous electric discharge systems. Several calculations have been made for mixtures of N_2 and CO to assess the effects of the relative N_2/CO concentrations on the CO vibrational kinetics and small-signal gain. These calculations assume that the discharge parameters, n_e and T_e, are not affected by changes in the relative concentrations of the two molecular species and thus isolate, perhaps artificially, the vibrational kinetics from the overall discharge kinetics. Such predictions are useful, however, in that they can help identify phenomena in the vibrational energy transfer processes which could be used to help meet particular objectives in a laser

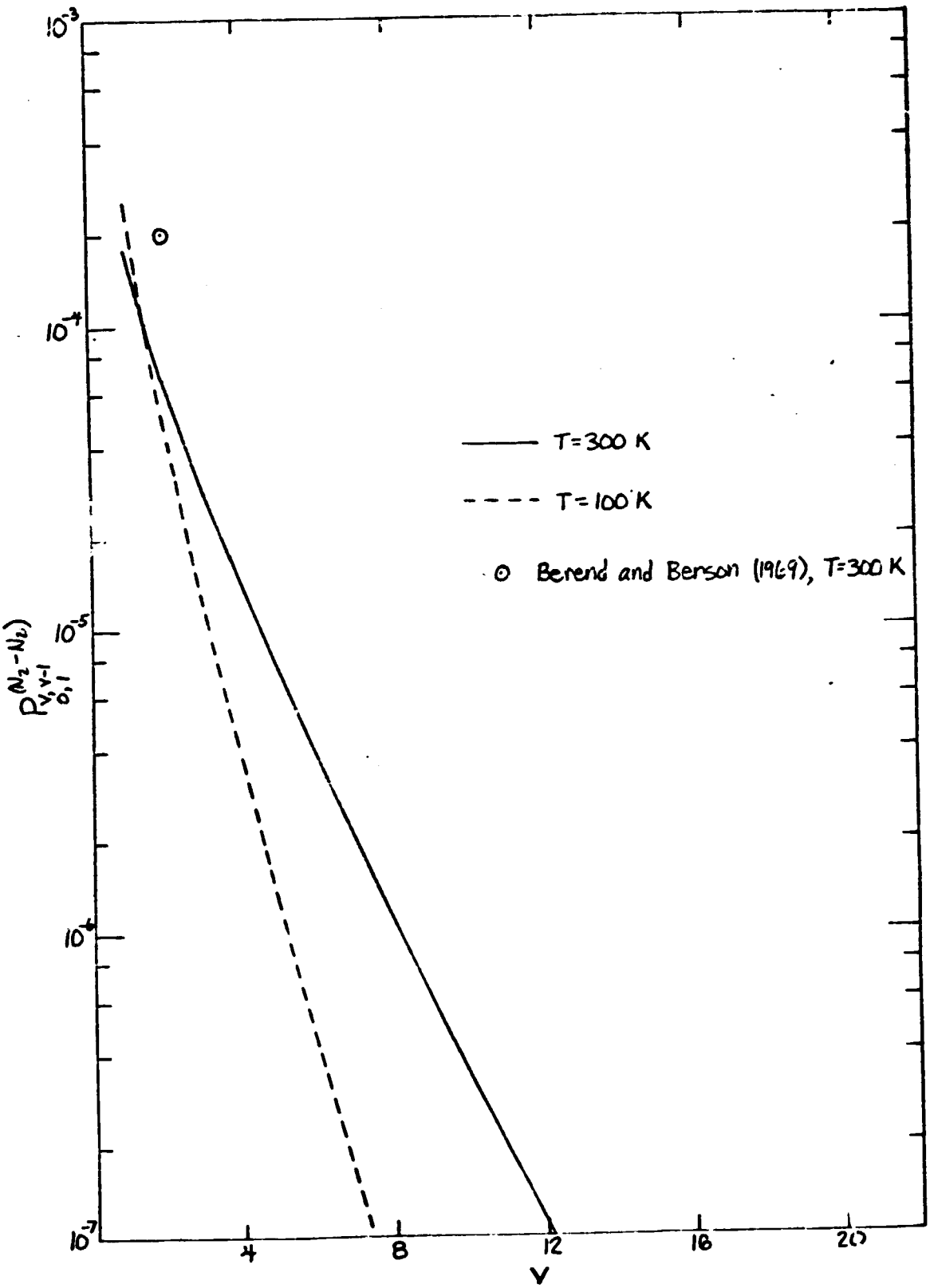

Figure 3. Calculated probabilities for the N_2-N_2 V-V exchange $N_2(v) + N_2(v=0) \rightarrow N_2(v-1) + N_2(v=1)$.

design, e.g. high gain in certain vibrational bands, changes in the delay time to maximum gain, etc.

Calculations for two mixtures of CO and N_2 are discussed in this section. The geometry and flow conditions for these calculations correspond to the small supersonic double-discharge system at Stanford. The flow channel in this system has a two-dimensional nozzle with an area ratio of 17.4. The total length of the test section is 30 cm, including the 20-cm discharge section and a 10-cm section downstream of the discharge. The sidewalls of the test section diverge uniformly to allow for boundary layer growth, with entrance and exit widths of 1.9 cm and 2.86 cm, respectively. The top and bottom walls of the discharge channel are formed by the flushed-mounted main discharge electrodes, which have a constant separation of 1.2 cm. Continuous supersonic flow in the test section is maintained by a diffuser and pump system with a volumetric capacity of 94 liters/sec.

For the calculations reported here stagnation conditions of 300 K and 4.06 atm were assumed. The calculated temperature and pressure in the test section for these conditions are approximately 65 K and 14 torr. The pressure calculation, which reflects boundary layer corrections to the one-dimensional isentropic flow equations, compares favorably with measured static pressures in the test section. Gas heating effects due to the discharge are included in the calculations.

Discharge conditions were assumed on the basis of an average current density of 10 mA/cm^2 and an estimated E/N of 2×10^{-16} $V \cdot cm^2$ for the main discharge. Solucions of the electron Boltzmann equation by Morgan and Fisher [12] and Nighan [13] were used to estimate the electron drift

velocity and average electron energy. The discharge parameters used in the calculations, based on these considerations, were $n_e = 2 \times 10^{10}$ cm^{-3} and $T_e = 7000$ K. If nearly all of the discharge energy is assumed to go into vibrational excitation, these values of electron number density and temperature lead to an energy loading $\leq 10^{-2}$ eV/molecule. This energy loading is consistent with the discharge performance attained in initial supersonic experiments with [illegible]en.

Stagnation and discharge conditions for the two calculations are summarized in Table 1.

Table 1. Discharge and stagnation conditions used in the calculations.

P_o, stagnation pressure	4.06 atm
T_o, stagnation temperature	300 K
n_e, electron number density	2×10^{10} cm^{-3}
T_e, electron temperature	7000 K

2.2.1 Case 1, N_2:CO = 90:10

The first calculation is for a mixture of 90% N_2, 10% CO. Results for the CO vibrational distribution and the maximum line-center gain coefficients are plotted in Figures 4 and 5. Distance on these graphs is defined from the beginning of the 20-cm discharge section. A temperature increase in the flow direction of approximately 3K is predicted due to gas heating effects. The calculated vibrational energy densities at the end of the discharge region are 2.5×10^{-2} eV/molecule for CO and 5.4×10^{-3} eV/molecule for N_2.

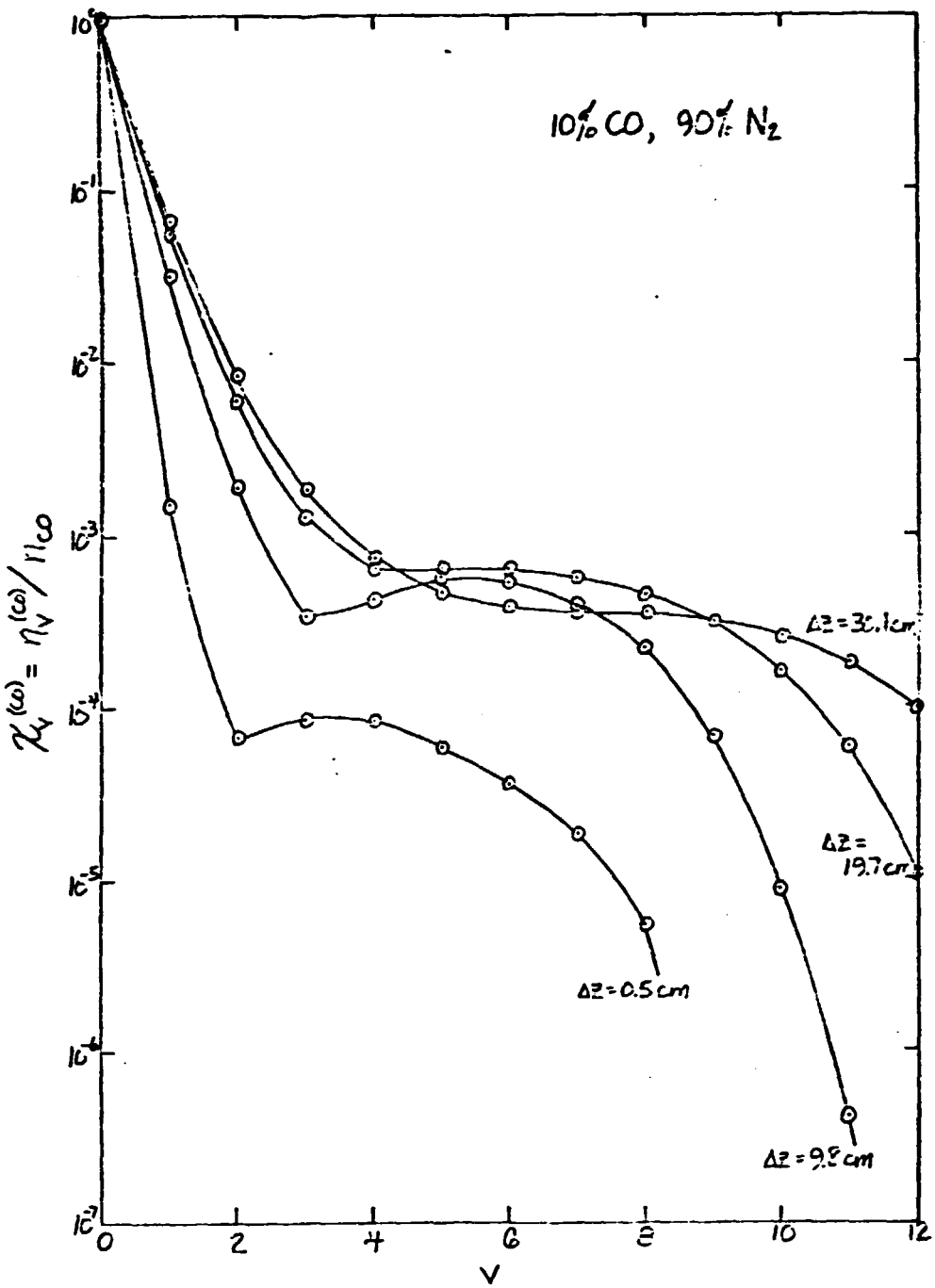

Figure 4. Normalized CO vibrational populations for Case 1, at four locations from the beginning of the discharge.

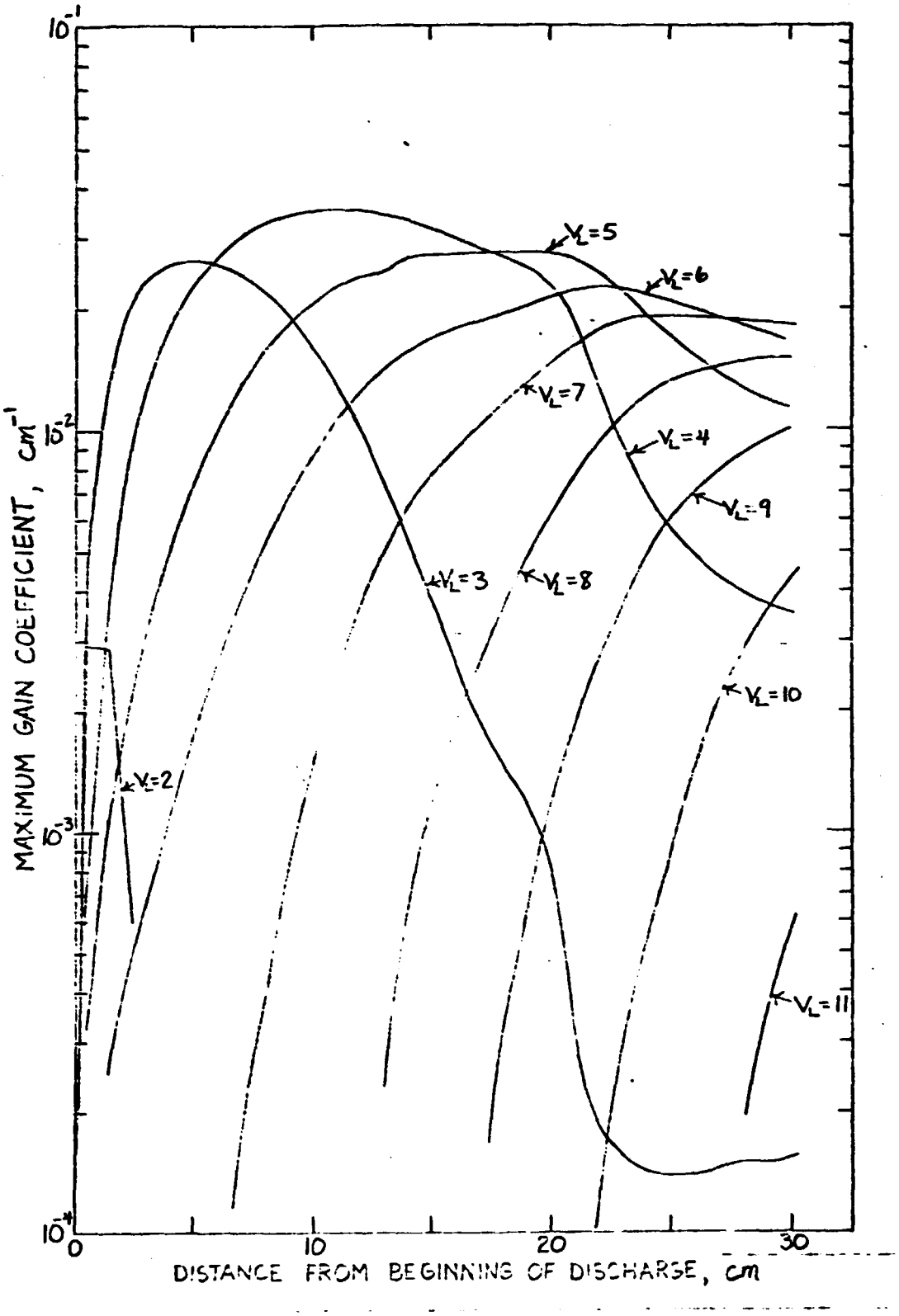

Figure 5. Maximum line-center gain coefficients for the CO laser transitions $V_L + 1 \rightarrow V_L$, Case 1.

The variation of the vibrational distribution and maximum gain coefficients with distance along the flow indicate that the CO-CO V-V processes dominate the vibrational energy transfer for this calculation. These effects are seen in the increase in gain of the higher-lying laser transitions at the expense of the gain on the lower transitions, representing an upward flow of vibrational energy. The net vibrational energy transfer in the interspecies V-V processes is from N_2 to CO, due to the smaller spacing of the CO vibrational energy levels. Most of this transferred energy is pumped into the low-lying CO levels, since the energy spacings for the lower levels are more nearly resonant with the N_2 energy spacings. This process is slow due to the small excited-level N_2 populations, and the transferred energy is quickly redistributed in CO by the faster CO-CO V-V processes. Although the probabilities for near-resonant V-V transfer in CO-CO and CO-N_2 are of similar magnitudes, the rates of transfer are also dependent on populations of vibrational levels which participate in the near-resonant transitions. For CO-CO collisions, these levels are adjacent and are rapidly populated through a "ladder"-climbing process, whereas for CO-N_2 collisions the near-resonant exchanges involve weakly-populated high-lying levels in N_2.

Total inversions are predicted at intermediate locations in the discharge for the $4 \rightarrow 3$ and $5 \rightarrow 4$ transitions. These inversions lead to significant gain for R-branch transitions. The P-branch and R-branch gain for the $4 \rightarrow 3$ vibrational band is plotted in Figure 6, for a distance of 5.5 cm into the discharge.

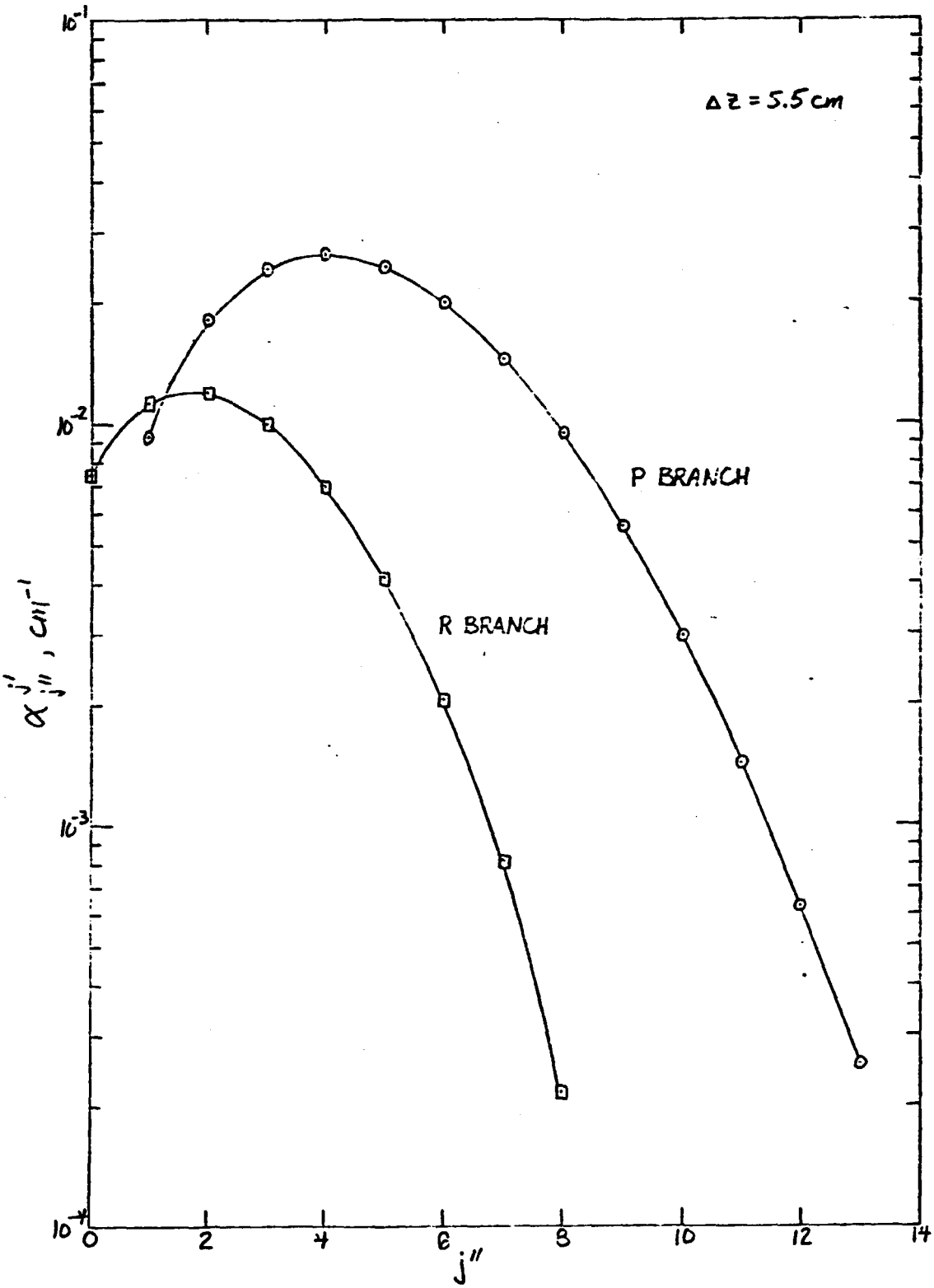

Figure 6. P-branch and R-branch gain coefficients at line center for the v = 4 → v = 3 vibrational band. The distance from the beginning of the discharge is 5.5 cm.

2.2.2 Case 2, N_2:CO = 98:2

The second calculation is for a mixture of 98% N_2 and 2% CO. The change in CO partial pressure from Case 1 causes a reduction by a factor of 5 in the CO-CO V-V transfer rate. This effect is evident in the calculated CO vibrational distribution, Figure 7, where the increase in population for the highest levels is slower than in the first calculation. The most striking difference in the calculated distributions for the two cases, however, is in the energy content, or average vibrational energy per CO molecule. At the end of the discharge, the vibrational energy densities for Case 2 are 5.8×10^{-2} eV/molecule for CO and 6.3×10^{-3} eV/molecule for N_2 . In the 10-cm section downstream of the discharge, the CO vibrational energy increases to 7.7×10^{-2} eV/molecule due to V-V transfer from N_2.

The higher vibrational energies in Case 2 are due to a greater energy storage capacity of the gas mixture. V-V transfer out of N_2 in CO-N_2 collisions, per molecule of N_2, is decreased due to the factor of 5 reduction in the CO concentration. At the same time, the rate of V-V energy transfer from N_2 into CO, per molecule of CO, is actually increased due to the slight increase in N_2 concentration. The result of these two effects is a higher CO vibrational energy, on a per-molecule basis.

The maximum gain curves for Case 2 are plotted in Figure 8. The overall magnitudes of the small-signal gain are generally lower than in Case 1, due primarily to the decreased CO concentration which results in lower population difference densities. The high gain for low-lying transitions in the early stages of the calculation is due to direct electron pumping. The increase in gain for these transitions farther downstream, particularly

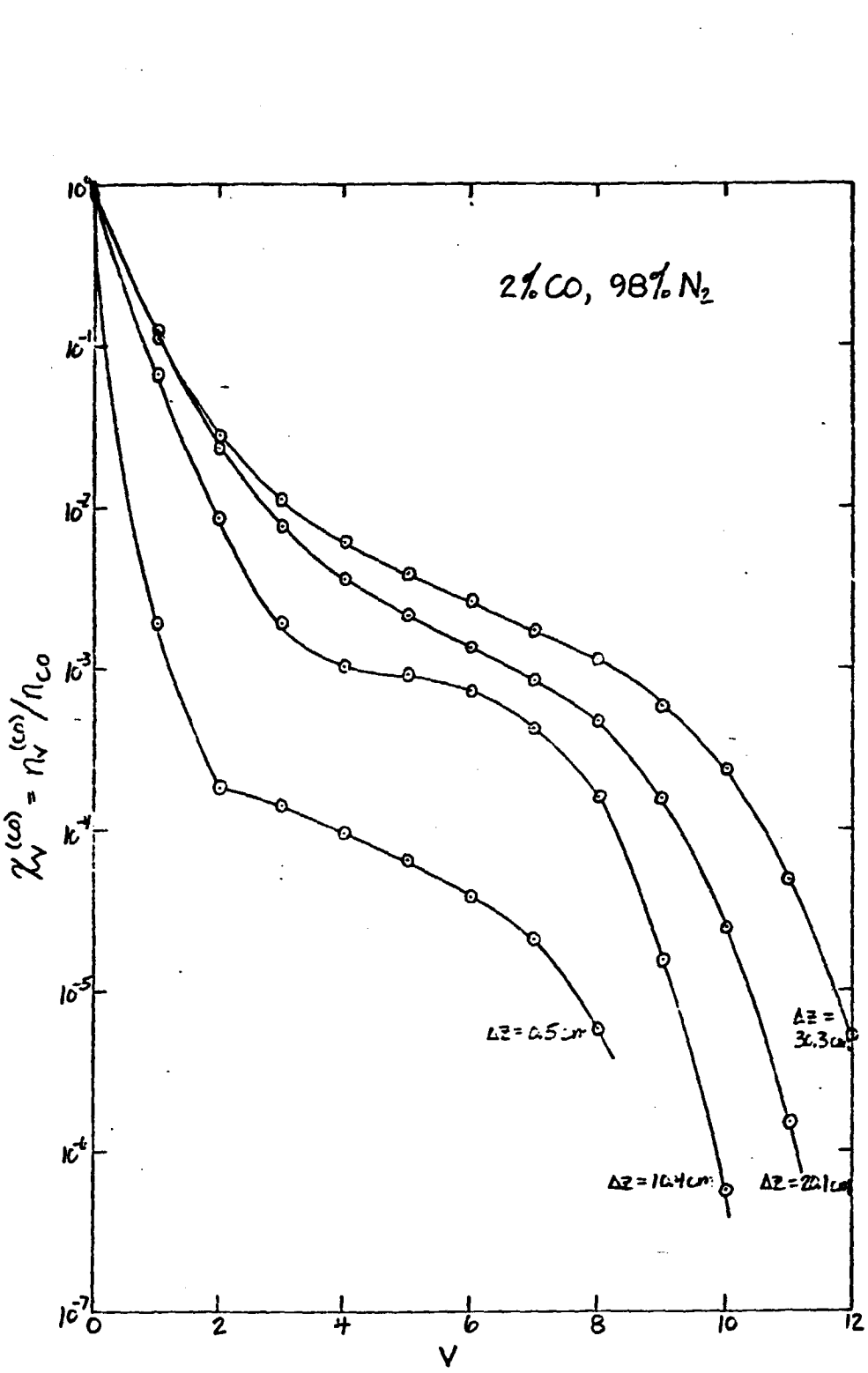

Figure 7. Normalized CO vibrational populations for Case 2.

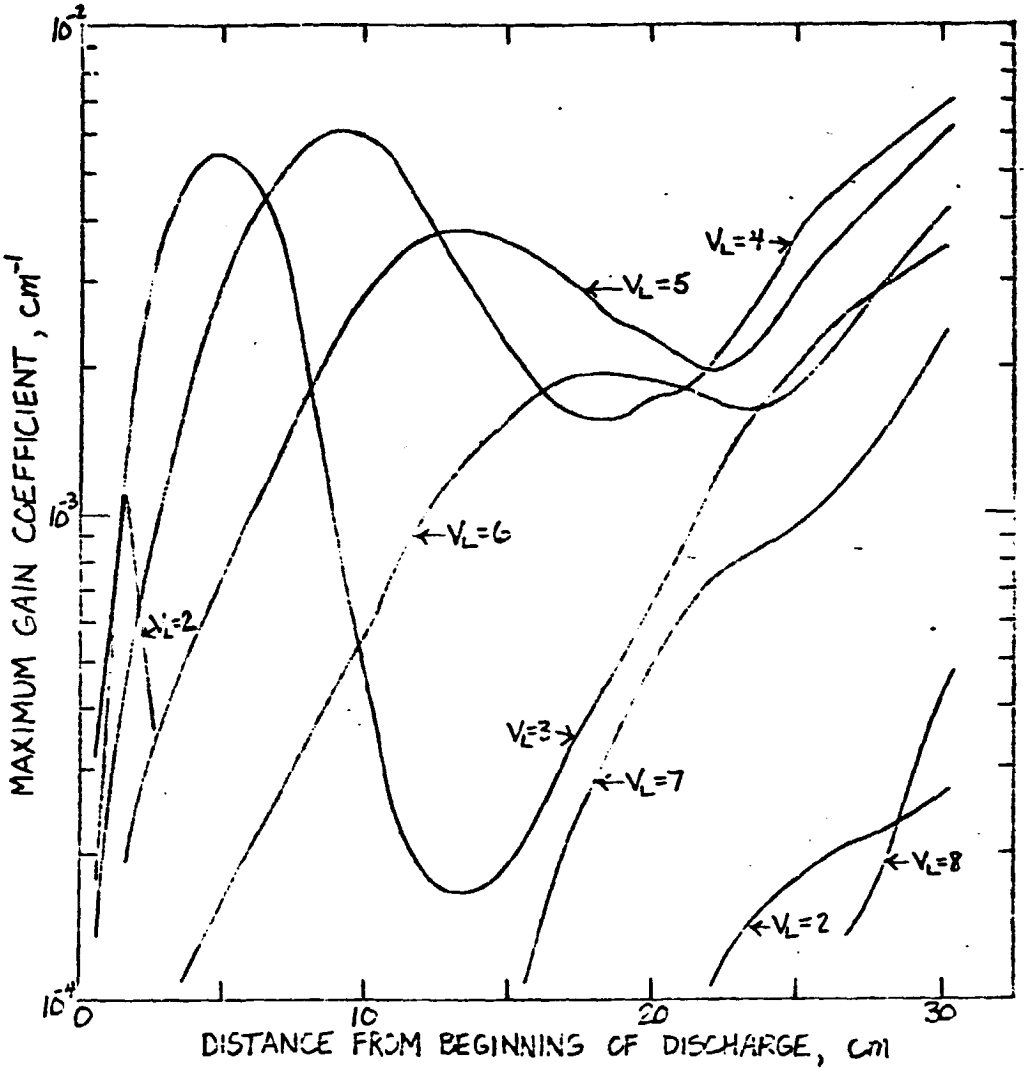

Figure 8. Maximum line-center gain coefficients for the CO laser transitions $V_L + 1 \rightarrow V_L$, Case 2.

beyond the discharge region, reflects the energy transfer from N_2 into the low-lying levels. This effect is of potential interest, because it may produce high gain for the low-lying transitions in a region downstream of the discharge, where the optical quality of the medium is perhaps improved. The phenomenon of delayed low-level gain enhancement due to V-V pumping by N_2 has also been observed in the CO laser kinetics calculations of Fisher [14].

3.0 LABORATORY STUDIES OF DOUBLE DISCHARGE

Experimental work during this six month period has continued to focus on the concept of the CW double discharge. In order to better conduct tests aimed at elucidating the discharge mechanism and increasing the electrical power loading, we have constructed a second-generation experimental facility. Although our available pump capacity limits the supersonic channel to the same cross-sectional dimensions employed in our first facility, the new facility has several improved design features and much greater flexibility. The basic design was described in our previous progress report. During the past six months the system has been assembled and tested for gasdynamic and electrical performance.

In summary, our experimental findings are as follows:

1. The cathode material was found to be an important factor in discharge performance, with copper performing better than aluminum.
2. Water cooling of the electrodes and improved mounting of pins has enabled operation at considerably higher pin currents than possible with the original test section.
3. The maximum electrical power loading (before arcing) was found to scale with the total pin current. At present we are power supply limited and cannot determine the maximum power loading achievable with total pin currents larger than 300 mA. We regard this effort to determine the dependence of maximum power loading with pin current to be a critical element of our study, and we are hopeful that the power loadings required for lasing can be achieved by operating with increased pin currents.

4. Preliminary tests with individually variable ballast resistors in the pin circuitry have confirmed that control of the individual pin currents can be used to improve discharge uniformity. Discharge uniformity and electrical power loading are of course both important in a practical device.

Recently we have ordered a new power supply to extend our operating range to higher power loadings. In the meantime, we have also made a major modification to the test section to allow injection of foreign gases into the cathode and anode boundary layers. This modification is motivated by our recognition of the role of photoionization in stabilizing the main discharge. Varying the gas in the vicinity of the cathode, where the photoionizing photons are created, should enable variation of the emission spectrum and hence of the volume ionization level in the core flow. At present, we are initiating tests to check the gasdynamic performance with injection. Subsequently, when the new power supply is installed, electrical tests will be conducted.

4.0 RESEARCH PLAN FOR NOVEMBER 1, 1975, TO APRIL 30, 1976.

During the forthcoming six-month period we plan to work on the following problems:

A. Laser Modeling

1. Parameter studies of system performance as a function of key variables such as gas composition, temperature, pressure, power loading and kinetics coefficients.
2. Addition of an option to include an optical cavity, if needed.
3. Development of a physical model for double discharge.

B. Laboratory Studies

1. Work to improve system performance, particularly the discharge uniformity and the power loading of the gas. Ideas include:
   a. Individual variable ballasting of pins in auxiliary discharge.
   b. Segmentation of anode for axial control of E/N in the main discharge.
   c. Studies at increased pin and main discharge currents, made possible with a new power supply.
   d. Electrode modifications, including rounding downstream edges of cathode and anode and masking anode sides to reduce breakdown through the warm sidewall boundary layers.
   e. Injection of gases into the cathode boundary layer, to stimulate UV emission or provide better heat dissipation.
   f. Variation in number, location and size of pins.

2. Work to improve understanding of double discharge:

   a. Investigate the role of photoionization

   b. Investigate the role of electrode materials and their characteristics such as work function, cathode voltage drop and material cleanliness and purity.

   c. Develop physical model of double discharge.

During the forthcoming year, we anticipate that our NASA-sponsored research will benefit from funding recently received from the National Science Foundation. These funds will allow us to improve and enlarge our experimental facilities for studies of discharges in supersonic flows. The overlap between the NASA- and NSF-sponsored research should benefit both programs, and in particular the increased size of our next test section, once installed, will enable more practical experiments than presently possible.

5.0 REFERENCES

[1] Sharma, R. D., "Vibration-to-Vibration Energy Transfer in CO-CO Collisions," Chem. Phys. Letters 30, 261-266 (1975).

[2] Hall, R. J., and Eckbreth, A. C., "Kinetic Modeling of CW CO Electric-Discharge Lasers," IEEE J. Quantum Electronics QE-10, 580-590 (1974).

[3] Smith, N. S., Hassan, H. A., and McInville, R. M., "Analysis of High-Flow Electric Discharge CO Laser Systems," Paper No. 74-180, AIAA 12th Aerospace Sciences Meeting, Washington, D.C., 1974.

[4] Shin, H. K., "Vibration-to Vibration Energy Transfer in Near-Resonant Collisions," J. Chem. Phys. 60, 1064-1070 (1974).

[5] Shin, H. K., "Vibration-to-Vibration Energy Transfer in N_2 + CO in the Temperature Region 100-3000°K," J. Chem. Phys. 61, 2474-2475 (1974).

[6] Stephenson, J. C., and Mosburg, E. R., "Vibrational Energy Transfer in CO from 100 to 300°K," J. Chem. Phys. 60, 3562-3566 (1974).

[7] Hancock, G., and Smith, I. W. M., "Quenching of Infrared Chemiluminescence. 1: The Rates of De-excitation of CO ($4 \leq V \leq 13$) by He, CO, NO, N_2, O_2, OCS, N_2O and CO_2," Applied Optics 10, 1827-1842 (1971).

[8] Zittel, P. F., and Moore, C. B., "Vibration-to-Vibration Energy Transfer in N_2-CO," Appl. Phys. Letters 21, 81-83 (1972).

[9] Green, W. H., and Hancock, J. K., "Measurement of CO(v=1) Vibrational Energy Transfer Rates Using a Frequency-Doubled CO_2 Laser," J. Chem. Phys. 59, 4326-4335 (1973).

[10] Green, W. H., and Hancock, J. K., "Laser-Excited Vibrational Energy Transfer Studies of HF, CO, and NO, " IEEE J. Quantum Electronics QE-9, 50-58 (1973).

[11] Berend, G. C., and Benson, S. W., "Vibration-Vibration Energy Transfer between Diatomic Molecules," J. Chem. Phys. 51, 1480-1484 (1969).

[12] Morgan, W. L., and Fisher, E. R., "Calculations on the Electron Energy Distribution in a Molecular Laser Plasma," Research Institute for Engineering Sciences Report RIES 74-56, Wayne State University, 1974.

[13] Nighan, W. L., "Electron Energy Distribution and Collision Rates in Electrically Excited N_2, CO, and CO_2," Phys. Rev. A 2, 1989-2000 (1970).

[14] Fisher, E. R., "Modeling of a Pulsed CO/N_2 Molecular Laser System, Part II: Effect of Mixture Components and Temperature Variation," Research Institute for Engineering Sciences Report RIES 72-48, Wayne State University, 1972.